EPRG-PRCI-APGA
23rd Joint Technical Meeting
Edinburgh, Scotland
6–10 June 2022

MECHANICAL DAMAGE FATIGUE AND FORMATION CRACKING ASSESSMENT TECHNIQUES
PAPER NUMBER: 20

Arnav Rana, Sanjay Tiku, Aaron Dinovitzer*,
BMT Canada Ltd., Ottawa ON, CA

Mark Piazza
American Petroleum Institute, Washington DC, US

Timothy Burns
Shell Midstream, Houston TX, US

* presenting author

ABSTRACT

Pipeline integrity management involves the application of pipeline condition information (e.g., pipe size, existence and size of features), operational/environmental conditions and line pipe material properties in engineering assessment (fitness-for-purpose) tools to evaluate operational risk. These assessments for mechanical damage rely heavily on ILI reported pipe condition relaying the geometry of the dent and interacting features. This work is reporting on results of the US Department of Transportation (US DOT) Pipeline and Hazardous Materials Administration (PHMSA) and Pipeline Research Council International (PRCI) mechanical damage research (PRCI MD 5-2) related to improvement of mechanical damage cracking assessment tools. This paper will present the details of the evaluation and enhancement of mechanical damage assessment tools to understand and control conservatism and uncertainty inherent in integrity management. This paper will describe a project and its results targeting mechanical damage assessment tools on three fronts including:

- Evaluation of dent formation strain prediction comparing full-scale test results with ASME (American Society of Mechanical Engineers) and ductile failure damage indicator (DFDI) dent formation strain limits demonstrating performance, conservatism and identifying opportunities for improvement,

- Evaluation of in-line inspection (ILI) feature measurement uncertainty impact on dent fatigue life estimation considering ILI performance trial data. This will consider data developed in ILI performance trials to define the impact of close to real world ILI measurement performance variability.

- Safety factor definition for previously developed PRCI and API RP 1183 dent fatigue life screening and analysis tools considering the confidence limits to assure conservatism of analysis results relative to full-scale testing, and

DISCLAIMER

attend the JTM and receive the Proceedings. The Proceedings and Papers may not be copied or circulated to organizations or individuals not authorized to attend the JTM. The Proceedings and the Papers shall be treated as confidential documents and may not be cited in papers or reports except those published under the auspices of EPRG, PRCI or APGA-RSC.

This work was funded in part, under the Department of Transportation, Pipeline and Hazardous Materials Safety Administration. The views and conclusions contained in this document should not be interpreted as representing the official policies, either expressed or implied, of the Pipeline and Hazardous Materials Safety Administration, the Department of Transportation, or the U.S. Government.

1. INTRODUCTION

The objective of the study presented in this paper was to evaluate and improve various aspects of mechanical damage integrity methodologies implemented in API 1183 [1]. The scope of present work encompassed the assessment and improvement of indentation strain prediction models, assessment of the effect of ILI data variability on fatigue life and strain estimations and quantification of safety factors inherent in different fatigue life estimation methodologies. Safety factors (modeling bias) defined in the present study and evaluated for different fatigue life estimation approaches in the present work refer to the conservatism inherent in different fatigue life models and is represented as the ratio of experimental lives to predicted lives. With regard to indentation strain estimation, the widely used ASME B31.8 strain model has been assessed against a large dent finite element (FE) database, and modifications have been presented to improve the accuracy of the estimated strains. Two indentation crack prediction criteria, DFDI [2][3] and ASME B31.8 Appendix R Limit Strain [4], have also been assessed with dent full-scale test results. The second area of interest investigated in this paper is the effect of ILI measurement variability on dent fatigue life and strain estimations. Two approaches have been adopted to understand this effect. First, Monte Carlo simulations were conducted by varying ILI dent profiles and the resulting effects on fatigue life and strain estimates were studied. Second, multiple ILI measurements of a set of dents from an ILI pull trial were employed to evaluate the fatigue life and strain estimate distributions. The final topic examined in this paper is the quantification of safety factors and associated certainty levels for various fatigue life assessment methods. This has been accomplished by fitting probability distribution functions to the data comparing experimental and predicted dent fatigue lives, and a method has been devised to scale these distributions to ensure certain factors of safety, at different confidence levels.

2. IMPROVEMENT OF INDENTATION CRACK FORMATION STRAIN ESTIMATES

Ductile damage in the form of cracking can be incurred during pipeline indentation. A method of assessing the level of damage incurred is to estimate the indentation strain from dent shape measurements and then comparing the calculated value against a defined “crack” formation strain. Various methodologies have been developed to predict the indentation strain [5][6][7], and of those, two were considered in this study – ASME B31.8 Appendix R Effective Strain and “Blade Energy Partners Simplified Model” Effective Strain, also referred to as ASME strain and Blade strain. The accuracy of the estimation of indentation strains was assessed against strain data from validated finite element (FE) analysis of dented pipes. Improvements to the ASME B31.8 criteria are proposed based on the observations made from these assessments. Additionally, accuracy of prediction of indentation strains for unrestrained dent shapes under pressure is also addressed and solutions are proposed to resolve this issue.

2.1. Dent Indentation Strain Estimation Models

The ASME and Blade strain estimation models considered in this project provide formulations of bending and membrane component strains in the axial and circumferential directions, at the dent

peak [2][4]. No formulation for circumferential membrane strain is offered in the ASME strain model, while it is present in the Blade strain model. In addition to the directional strains, an effective or total strain formulation has also been provided. This effective strain is a scalar measure of triaxial strain.

2.1.1. ASME B31.8 Appendix R – 2018 Model

The strain formulations as provided in ASME B31.8 Appendix R (2018), are as follows [4],

$$\varepsilon_1 = \left(\frac{t}{2}\right)\left(\frac{1}{R_0} - \frac{1}{R_1}\right) \tag{1}$$

$$\varepsilon_2 = \left(\frac{t}{2}\right)\left(\frac{1}{R_2}\right) \tag{2}$$

$$\varepsilon_3 = \left(\frac{1}{2}\right)\left(\frac{d}{L}\right)^2 \tag{3}$$

$$\varepsilon_{eff} = \left(2/\sqrt{3}\right)\left[\,\varepsilon_1^2 + \varepsilon_1\,(\varepsilon_2 + \varepsilon_3) + (\varepsilon_2 + \varepsilon_3)^2\,\right]^{1/2} \tag{4}$$

Where, t is the pipe wall thickness, R_0 is the pipe nominal outer radius, R_1 is the radius of curvature of the circumferential dent profile at the dent apex, R_2 is the radius of curvature of the axial dent profile at the dent apex, d is the depth of the dent, L is the length of the dent, ε_1 is the circumferential bending strain, ε_2 is the axial bending strain, ε_3 is the axial membrane strain and ε_{eff} is the effective strain.

2.1.2. Blade Energy Partners Simplified Model

In the Blade strain model, the bending strain formulations are the same as that offered by ASME B31.8. The membrane strain formulations, both axial and circumferential, are based on evaluating the change in the length of an undeformed segment near the dent apex, brought upon by the rotation induced by bending [2]. This can account for the membrane strain induced by rotation but not for the in-plane extension. For the axial membrane strain, a method for evaluating the in-line extension was used based on the work of Rosenfeld [7]. The membrane strain equation is as follows [2],

$$\varepsilon = (L_s - L_0) \,/\, L_0 \tag{5}$$

Where, L_S is the deformed length and L_0 is the undeformed length of a span near the dent apex. Since the circumferential strain is also present, the effective strain formulation is as follows,

$$\varepsilon_{eff} = \left(2/\sqrt{3}\right)\left[(\varepsilon_1 + \varepsilon_4)^2 + (\varepsilon_1 + \varepsilon_4)\,(\varepsilon_2 + \varepsilon_3) + (\varepsilon_2 + \varepsilon_3)^2\,\right]^{½} \tag{6}$$

Where, ε_4 is the circumferential membrane strain, while the remaining variables are as described in Equation (1) to (4).

2.2. Assessment of Indentation Strain Estimates

For comparison of ASME and Blade estimated strains with strains from finite element dent modeling, geometry and strain data were extracted from the validated BMT FE Dent Database [8][9]. The database consists of hypothetical dents, as well as FE models of dent full-scale tests and in-service field dents. FE models of about 4600 hypothetical dents, 60 full-scale test dents and 100 in-service field dents at indentation were used to assess the strain estimates against the FE strains. The FE indentation database consisted of dents created under a wide range of conditions pertaining to pipe geometry (outer diameter (OD) 114-1066 mm/4-42 in), dent depth (0.5-10% OD), indentation pressure (0-90% PSMYS) and indenter type (spherical, elliptical, transverse bar of various sizes). For more details on the indentation FE database, please refer to Ref [8]. For more details regarding full-scale tests, please refer to Ref [10][11][12].

The assessment process involved the extraction of axial and transverse dent profiles through the dent apex from the dent geometry data and the evaluation of required geometric quantities (curvature, depth, length) about the dent apex for calculation of ASME and Blade strains. The component strains at the dent peak were extracted from the FE models and the equivalent strains were calculated. The equivalent strain is analogous to the effective strain used in strain estimation models [3][13]. The FE equivalent strain can be calculated from the norm of the deviatoric components of strain (Equation 7 and 8) [13]. For more details regarding the process of evaluating the strain estimates from the geometry data please refer to Ref [8].

$$dev(\varepsilon_{ij}) = \varepsilon_{ij} - \frac{1}{3}\, trace(\varepsilon_{ij})\delta_{ij} \tag{7}$$

$$\varepsilon_{eq} = \sqrt{(2/3)\, dev(\varepsilon_{ij})\, dev(\varepsilon_{ij})} \tag{8}$$

2.2.1. Comparison of ASME strain against FE strain

Comparison of the ASME and FE effective strains showed good agreement, with 76% of hypothetical, 82% of full-scale and 79% of field dent data falling within a 20% error band. The unity plots comparing the ASME effective strain against the FE equivalent strains for full-scale, field and hypothetical dents are given in Figure 1. From Figure 1(c), it can be observed that for several data points, the ASME strains significantly diverge from the corresponding FE values. These data points belong to deep (>= 6% OD) dents with sharp radii (radii of curvature of dent peak <200 mm/8 in) subjected to high indentation pressures (>= 60% PSMYS). Deep indentation at high pressures produces significant plastic damage in the form of high axial and circumferential membrane strains at the dent apex. It was found that the ASME axial membrane strain formulation significantly underpredicted the axial membrane strain [8] and additionally, there is no formulation to predict circumferential membrane strain in ASME B31.8 model. This results in the ASME effective strains underpredicting when compared to the FE equivalent strains in these cases. The unity plot of ASME vs FE strain of hypothetical dents without the deep and sharp dents is presented in Figure 2. Here, it can be observed that the data points are in good agreement.

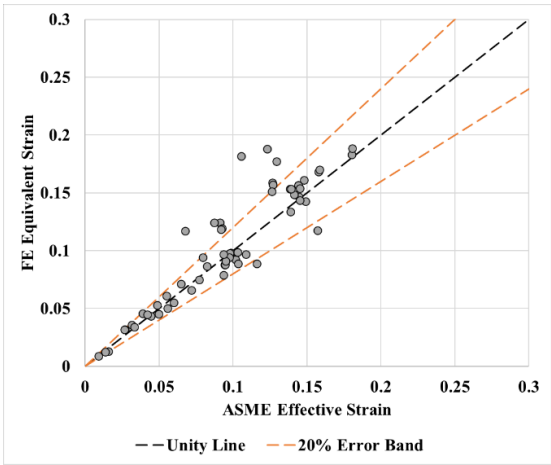

(a)

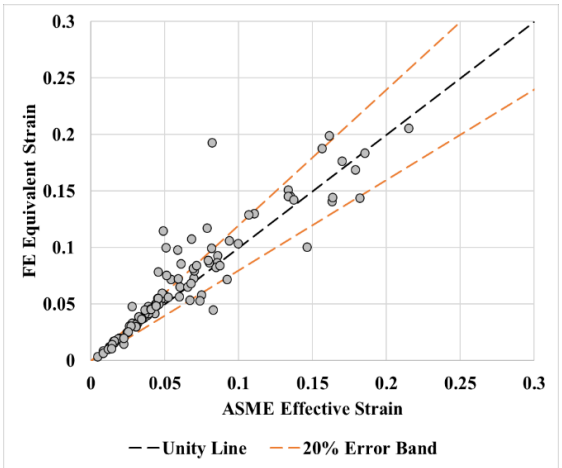

(b)

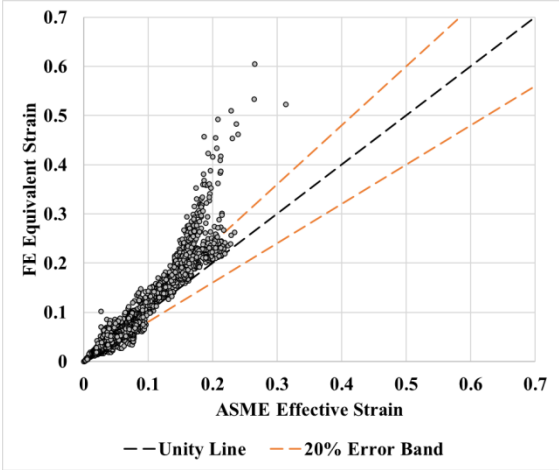

(c)

Figure 1 - Unity plots of ASME effective strain vs FE equivalent strain calculated using FE models from (a) full-Scale (b) field dents (c) hypothetical dents

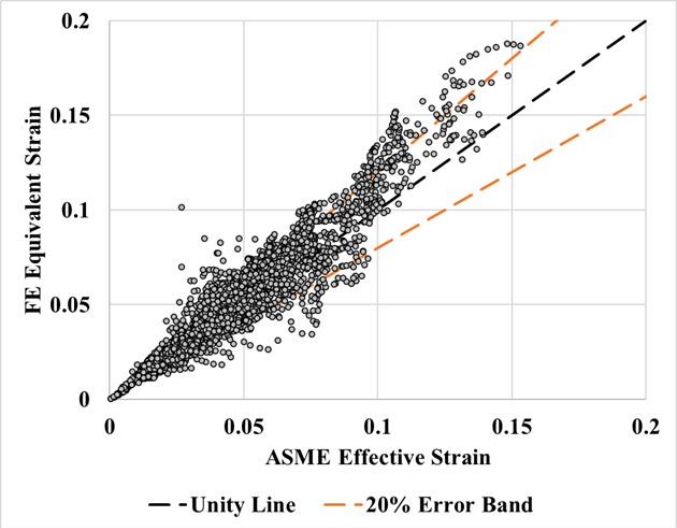

Figure 2 - Unity plot of ASME effective strain vs FE equivalent strain for hypothetical dents without the deep and sharp dents

2.2.2. Comparison of Blade strain against FE strain

Comparison of the Blade effective strains against the FE equivalent strains showed good agreement, with 86% of hypothetical, 83% of full-scale and 77% of field dent data falling within a 20% error band (Figure 3). Furthermore, the accuracy of effective strain estimates for deep and sharp dents is significantly improved over the ASME estimates as can be observed by comparing Figure 1(c) and Figure 3(c). This can be attributed to the presence of a circumferential membrane strain formulation and the improved axial membrane strain formulation.

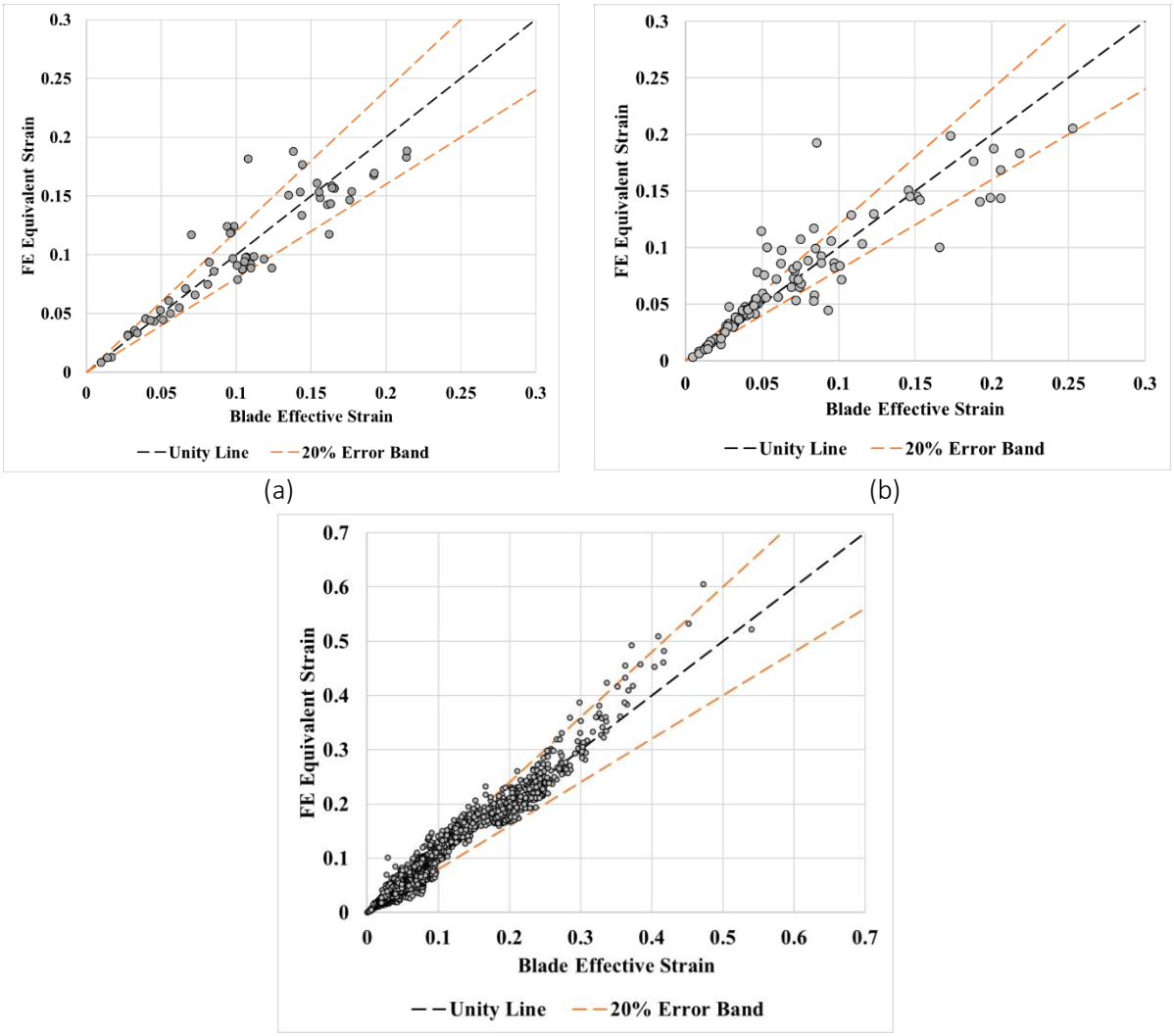

Figure 3 - Unity plots of Blade effective strain vs FE equivalent strain calculated using FE models from (a) full-scale (b) field dents (c) hypothetical dents

2.3. Prediction of Indentation Strains for Restrained and Unrestrained Dents Measured under Pressure

The strain estimates evaluated in the previous section have been used to predict strains in the FE models of dents at indentation. The dent geometry used for these evaluations were extracted at the indentation step. ILI measurements of the dents may or may not represent the dent shape at indentation. For a restrained dent, the indenter (rock) is in place and the shape will be consistent with the shape at indentation, but this is not the case for unrestrained dents. The removal of the indenter and application of pressure can cause significant re-rounding for unrestrained dents. This can be observed in the example shown in Figure 4. The figure shows an example of a dent after indentation and indenter removal that has been subjected to a maximum pressure (e.g., hydro test) after indenter removal and the shape is then measured at different mean pressures (e.g., ILI run pressure). The removal of the indenter and the application of pressure has significantly altered the shape of the dent from the indentation shape. Therefore, dent strain calculations performed on an unrestrained dent based on ILI data does not represent dent indentation strain.

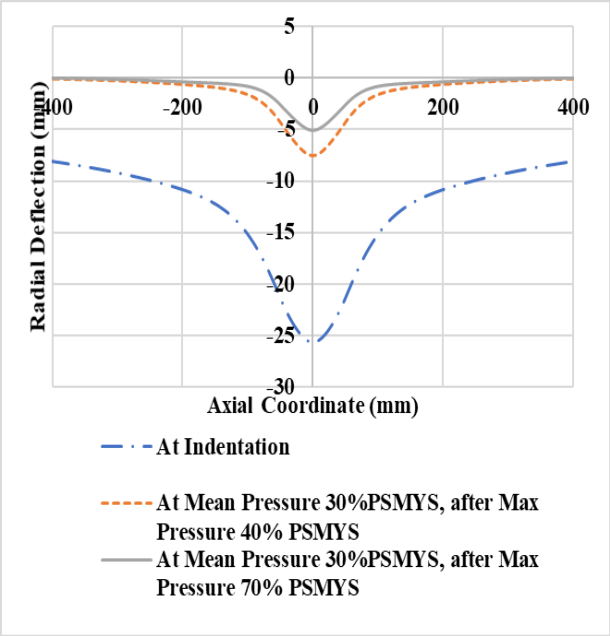

Figure 4 – Dent axial profiles at indentation and after re-rounding

ILI measurements of restrained dents reflect the shape at indentation, hence the strain estimates calculated using these measurements would reflect the indentation strain values. This can be observed in Figure 5(a), for hypothetical restrained FE dents where the strain estimates from shape measured at pressure (ILI measurement) and shape at indentation are compared. Most of the data points are in good agreement. For hypothetical unrestrained FE dents, the strains evaluated using shape at pressure and at indentation are not in good agreement (Figure 5(b)) as suggested by the significant re-rounding experienced by the unrestrained dent in the example in Figure 4. The strain estimates evaluated after indenter removal, at pressure are significantly underpredicted compared to indentation strain values.

For unrestrained dents, it was observed that the re-rounded shape and the resulting strains were primarily dependent on the maximum pressure experienced by the dent. The maximum pressure applied after indenter removal defines the final shape of the dent, and lower pressures after the dent shape has stabilized do not greatly alter the unrestrained dent shape. This can be inferred from the relative overlap of data sets in Figure 5(b) evaluated at different lower mean pressures after the dents experienced the same higher pressure. The effect of pressure on the strain estimates of unrestrained dents can be observed in Figure 6. In the figure, the ASME strains evaluated using dent shape at a pressure are compared against the ASME strains evaluated at indentation. In this case, dents have not seen a prior higher pressure. The shapes of the dents have been measured at the same pressure (30% PSMYS), but the three sets of dents have experienced different pressures after indenter removal, which has resulted in significant differences of shapes, hence the strain estimates. Application of larger pressures induce greater reduction in dent peak curvatures resulting in significant underprediction of strain compared to indentation values.

The hypothetical dent database mentioned earlier was used for the assessment of strain estimates for restrained and unrestrained dents. The dents after indentation were subjected to various maximum pressures (20-90 %PSMYS) and lower mean pressures (10-80 %PSMYS), resulting in about 98,000 and 24,000 FE cases for restrained and unrestrained dents, respectively. In conclusion, it can be stated that the presence or absence of indenter and the maximum pressure applied to the dent play a critical role in the final shape of the dents. For restrained dents, due to the presence of the indenter, the final shapes do not alter greatly from the shapes at indentation, hence strains evaluated using the final shapes mostly do reflect the indentation strains. In contrast, for unrestrained dents the removal of indenter and application of pressure greatly deviates the dent shapes away from the shapes at

indentation, hence resulting in the strain estimates made using the final dent shapes to not reflect the indentation strain.

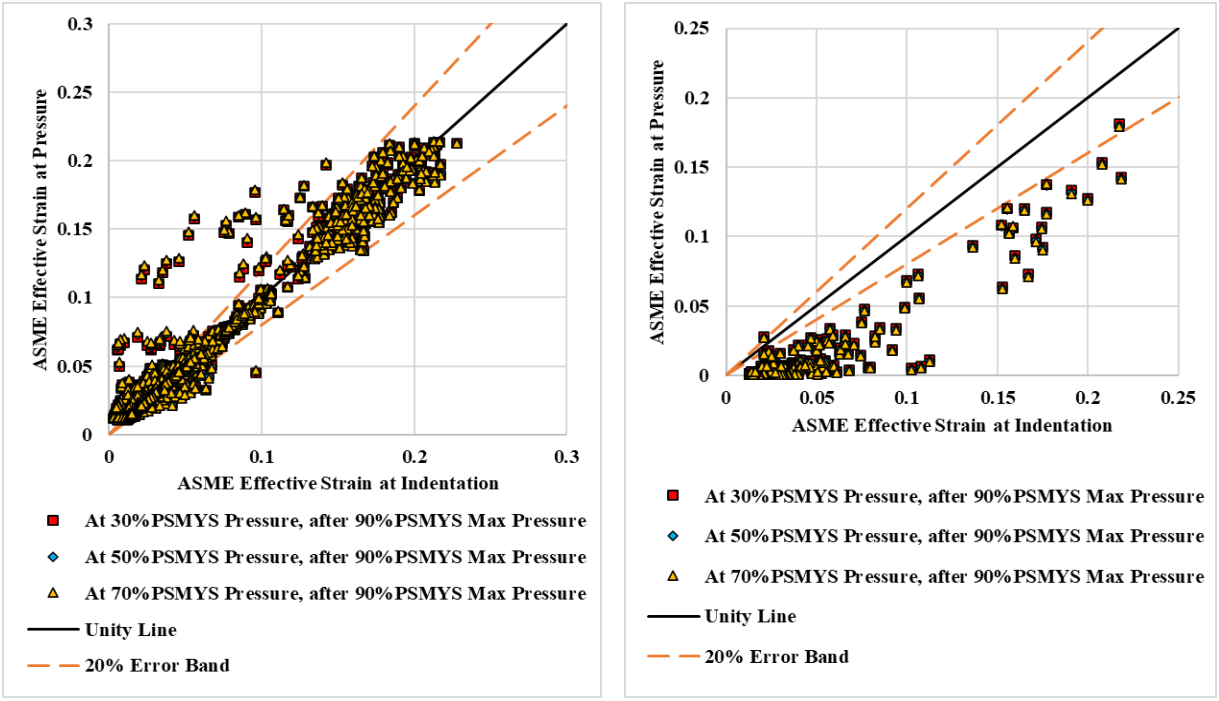

Figure 5 - Comparison of ASME Strain Estimates Evaluated from Hypothetical (a) Restrained and (b) Unrestrained Dent Shapes at Pressure and Indentation

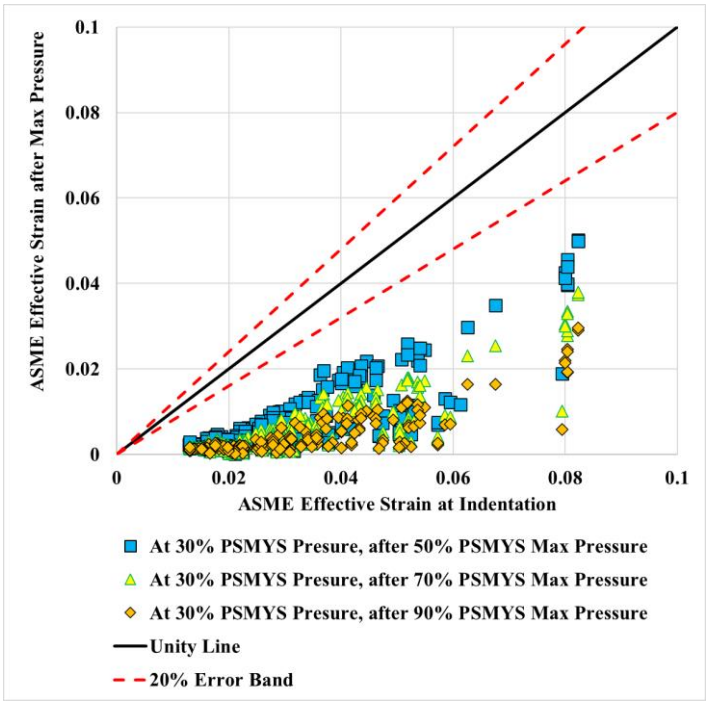

Figure 6 - Comparison of ASME strains at indentation vs ASME strains of unrestrained dents after experiencing various maximum pressures

2.4. Improvements to ASME B31.8 Strain

Two aspects were explored for the improvement of indentation strain prediction. First, was the improvement of the membrane strain formulations (axial and circumferential) and the second, was pertaining to prediction of indentation strain for unrestrained dents measured at pressure.

2.4.1. Modification of ASME Axial Membrane Strain Formulation

As mentioned in section 2.2.1, it was observed that the ASME membrane strain formulation significantly underpredicted when compared to FE strains. The current formulation is based on right-angled triangle approximation of the dent to estimate the deformed length of the dent profile. Performing that derivation yields a formulation with a coefficient of 2 instead of ½. This had been pointed out earlier as well [5]. Additionally, no guidance has been provided with regard to the reference length and depth to be used for evaluating the strain. Using references far from the dent peak leads to overestimation of length and hence significant under prediction of strain. Several references were considered, and it was found that the depth and length from the 85% dent depth reference (as per API 1183 [1]) were suitable (Figure 7).

$$\varepsilon_3 = 2\left(d/L\right)^2 \tag{9}$$

Where, d and L are reference depth and length at 85% dent depth. Please refer to Ref [8] for more information regarding extraction of the reference depth and length.

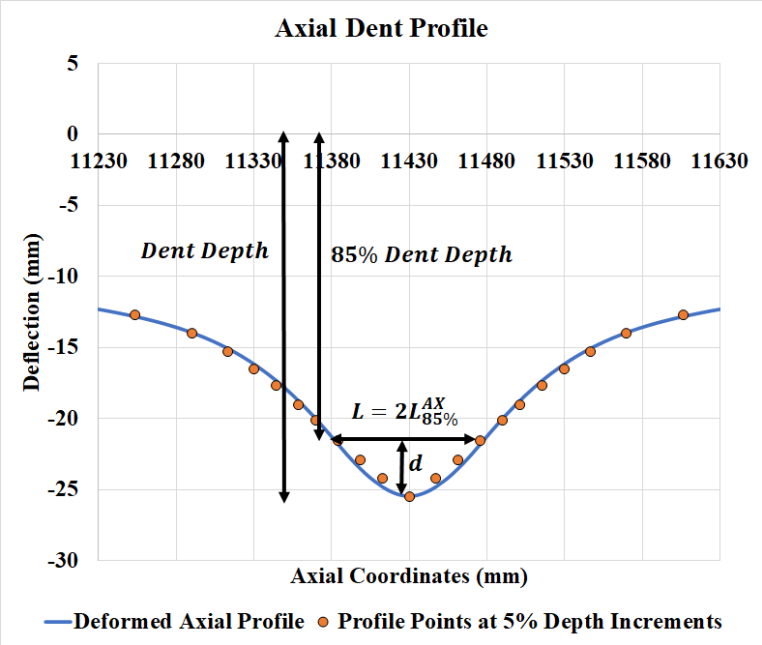

Figure 7 - Reference for evaluating modified ASME axial membrane strain

2.4.2. Modification of ASME Circumferential Membrane Strain Formulation

ASME strain does not have a circumferential membrane strain formulation, therefore, a formulation was devised based on a framework similar to that of the axial membrane strain. The formulation is based on predicting the membrane strain by comparing the deformed and undeformed lengths about the dent peak, using linear distance approximation to evaluate the arc lengths. The first step requires extracting a circumferential deformed span about the dent peak. The radial distance of the peak is represented by r_p, and the radial distance of an end of the span as r and the angular distance of that end away from the peak as θ.

$$
\begin{aligned}
L_S &= \sqrt{r^2 + {r_p}^2 - 2\, r\, r_p\, \cos\theta} \\
L_0 &= r\sqrt{2(1 - \cos\theta)} \\
L_{def} &= L_S\, cw + L_S\, ccw \\
L_{undef} &= L_0\, cw + L_0\, ccw \\
\varepsilon_4 &= \left(L_{def} - L_{undef}\right) / L_{undef}
\end{aligned}
\tag{10}
$$

Where, L_S and L_0 are the deformed and undeformed lengths, respectively. These values must be evaluated for both clockwise and counter-clockwise directions and then summed to get the total deformed (L_{def}) and undeformed (L_{undef}) lengths. As in the case of axial membrane strain, the judicious selection of the span about the peak is required for better approximation of the strain. For the assessment of the modified model, the points on the circumferential profile associated with 85% dent depth (as per API RP 1183) were taken as the ends of the span about the dent peak (Figure 8). Please refer to Ref [8] for more information regarding extraction of the deformed and undeformed spans.

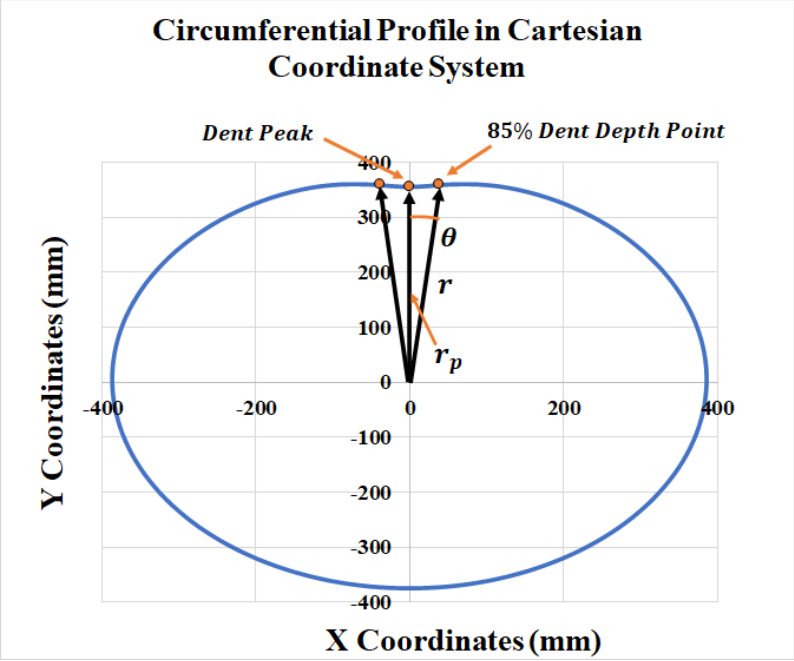

Figure 8 - Deformed circumferential profile and extracted span for membrane strain calculation

2.4.3. Assessment of Modified ASME Model

Similar to the assessments of ASME and Blade strains, the modified ASME effective strains calculated using Equation 6, by employing membrane strains from Equation 9 and 10, were compared against the FE equivalent strains and were found in good agreement, with 82% of hypothetical, 80% full-scale and 75% field dent data falling within 20% error band (Figure 9). The strain estimates of the deep and sharp hypothetical dents compared well against the FE values, a significant improvement over ASME strains (Figure 9(c)).

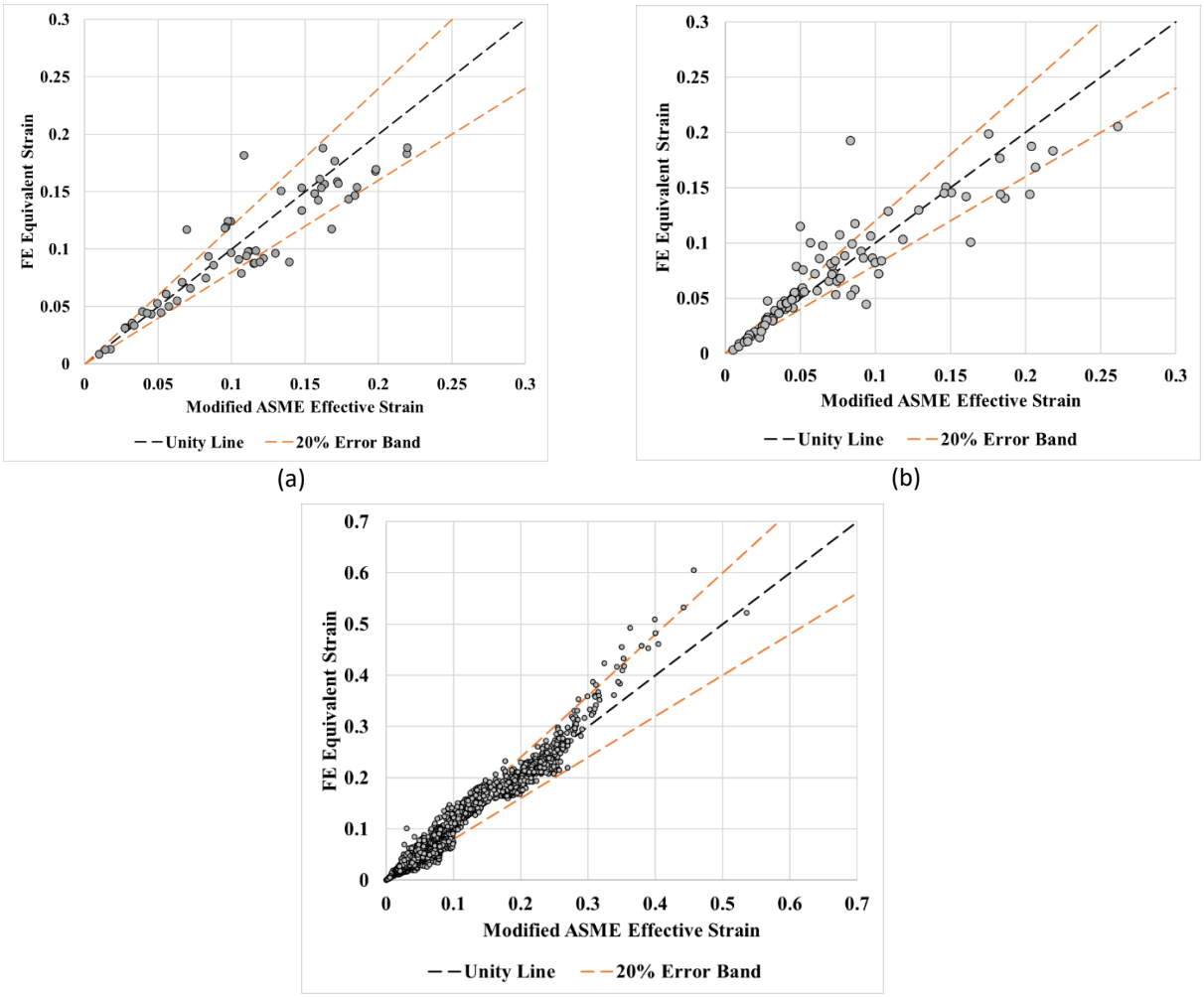

Figure 9 - Unity plots of modified ASME effective strain vs FE equivalent strain calculated using FE models from (a) full-scale (b) field dents (c) hypothetical dents

2.4.4. Prediction of Indentation Strains for Unrestrained Dents

As discussed in section 2.3, for unrestrained dents the shape measured at pressure does not represent the indentation shape. A regression model was devised where the effective strain evaluated using dent shape measured at pressure can be used to predict the effective strain at indentation. The curve fitting was accomplished using the *lsqnonlin* MATLAB function, which is a nonlinear least squared regression tool [14].

$$\begin{aligned} E_I &= c_1 * E_P + c_2 * E_P^{|c_3|} \\ c_1 &= b_1 + b_2 * Pmax + b_3 * Pmean + b_4 * OD/WT \\ c_2 &= b_5 + b_6 * Pmax + b_7 * Pmean + b_8 * OD/WT \\ c_3 &= b_9 + b_{10} * Pmax + b_{11} * Pmean + b_{12} * OD/WT \end{aligned} \quad (11)$$

Where, E_I is the predicted effective strain at indentation, E_P is the effective strain evaluated from the unrestrained dent shape at pressure, $Pmean$ is the mean pressure at ILI measurement of dent shape as percentage of P_{SMYS}, $Pmax$ is the maximum pressure experienced by the dent as percentage of P_{SMYS} and *OD/WT* is the ratio of pipe outer diameter to wall thickness. This predictive equation can be employed for ASME and modified ASME models. The coefficients b_i's for ASME and modified ASME strains are given below in Table 1.

Coefficients	ASME Strain	Modified ASME Strain
b1	8.0397E-01	7.0567E-01
b2	-2.1443E-05	1.9833E-03
b3	-4.8577E-04	1.1354E-04
b4	1.5435E-03	3.126E-03
b5	3.4513E-02	2.6672E-02
b6	3.6336E-04	4.2429E-04
b7	7.8631E-05	8.3458E-05
b8	-2.9772E-04	-2.2784E-04
b9	2.1983E-02	-3.0317E-02
b10	1.8032E-05	1.7133E-05
b11	-1.2964E-06	2.4208E-06
b12	-9.801E-04	1.2294E-03

Table 1 - Coefficients in Equation 11

The goodness-of-fit of the prediction model can be observed in Figure 10, where the indentation ASME and modified ASME effective strains predicted by Equation 11, using the shape evaluated at pressure, are compared against the ASME and modified ASME effective strains evaluated from the FE shape at indentation. Seventy-three percent (73%) and 77% of data points fall within a 20% error band for ASME and modified ASME strain indentation strain prediction models, respectively. About 23,000 data points were used to perform the fitting. Additionally, a set of 55 unrestrained dent FE models from the full-scale test database was used to test the regression equations. When the predicted indentation effective strains were compared against the effective strains evaluated at indentation, 81% and 82% of data points fell within the 20% error bands for ASME and modified ASME models (Figure 11).

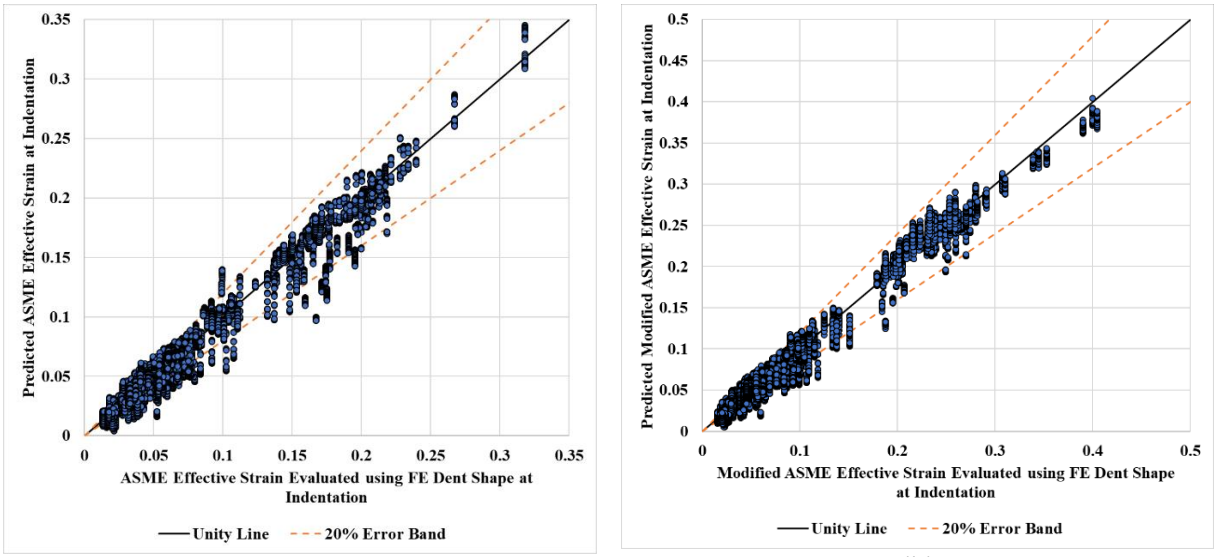

(a) (b)

Figure 10 – (a) ASME effective strain at indentation predicted by Equation (11) vs the ASME effective strain evaluated using FE dent shape at indentation (b) modified ASME effective strain at indentation predicted by Equation (11) vs the modified ASME effective strain evaluated using FE dent shape at indentation. Data set used for training.

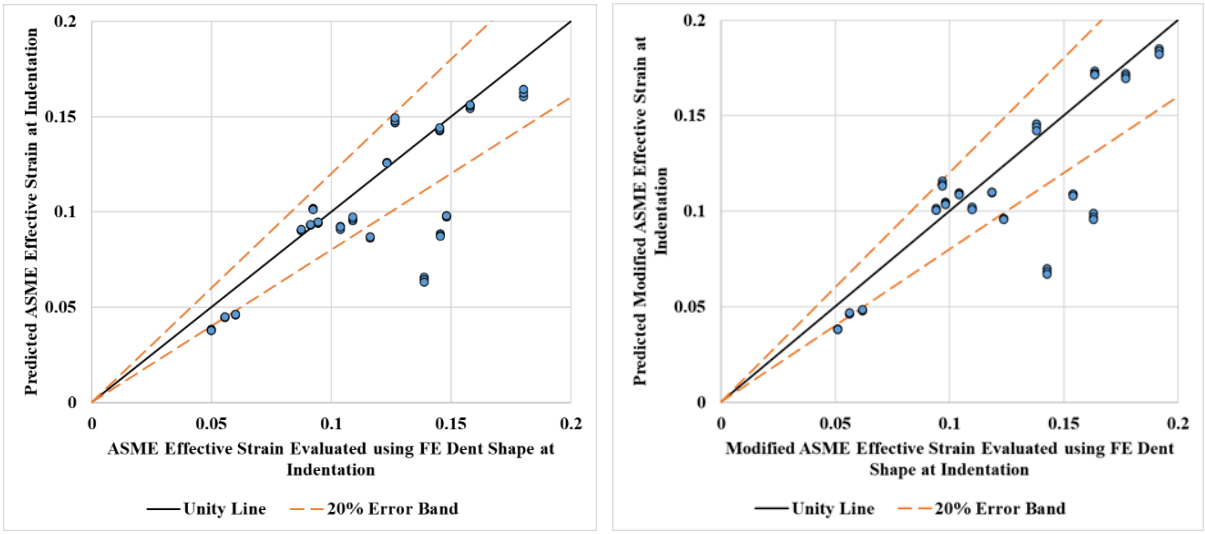

(a) (b)

Figure 11 – (a) Unity plot comparing predicted ASME effective strain at indentation vs ASME effective strain evaluated using FE dent shape at indentation (b) Unity plot comparing predicted modified ASME effective strain at indentation vs modified ASME effective strain evaluated using FE dent shape at indentation. Data set used for testing regression equation.

2.5. Dent Strain Cracking Criteria

In this section, two dent strain cracking criteria DFDI and ASME B31.8 Limit Strain have been compared against full-scale test results.

2.5.1. Ductile Failure Damage Indicator (DFDI)

DFDI is a ductile damage prediction index which predicts the onset of cracking due to ductile damage. The more detailed formulation of DFDI is a function of equivalent strain and stress triaxiality and is required to be integrated across the deformation history [15]. A simplified upper bound screening formulation of the DFDI index was adopted [2][3].

$$DFDI_{Upper\ Bound} = \frac{1.65\varepsilon_{eq}}{\varepsilon_0} \tag{12}$$

Where, ε_{eq} is the equivalent strain, ε_0 is a material property called critical strain which represents crack inception true strain under uniaxial testing. The evaluated indentation effective strains can be used as the equivalent strain to estimate the state of damage incurred by the pipe due to indentation[2][3]. The critical strain for pipeline materials is usually between 0.3 to 0.5 [2]. DFDI index = 0 represents the undamaged state, while DFDI index = 1 represents the damaged state. A damage limit of DFDI = 0.6 can be employed and has been suggested as a conservative option [2]. The upper bound DFDI was evaluated for 47 dents involved in the full-scale tests. These values were evaluated using the ASME, Blade and modified ASME strains. Based upon the least conservative option (critical strain (ε_0) = 0.5, DFDI cracking limit = 1) 0 dents were predicted to have incurred cracking during indentation for these models. While the most conservative option (critical strain (ε_0) = 0.3, DFDI cracking limit = 0.6) predicted 15, 16 and 21 cracks, respectively. None of the full-scale tests had incurred cracking during indentation. The DFDI indices for the 47 dents calculated using ASME, Blade and modified ASME strains and critical strain of 0.3 and 0.5, are presented in Figure 12.

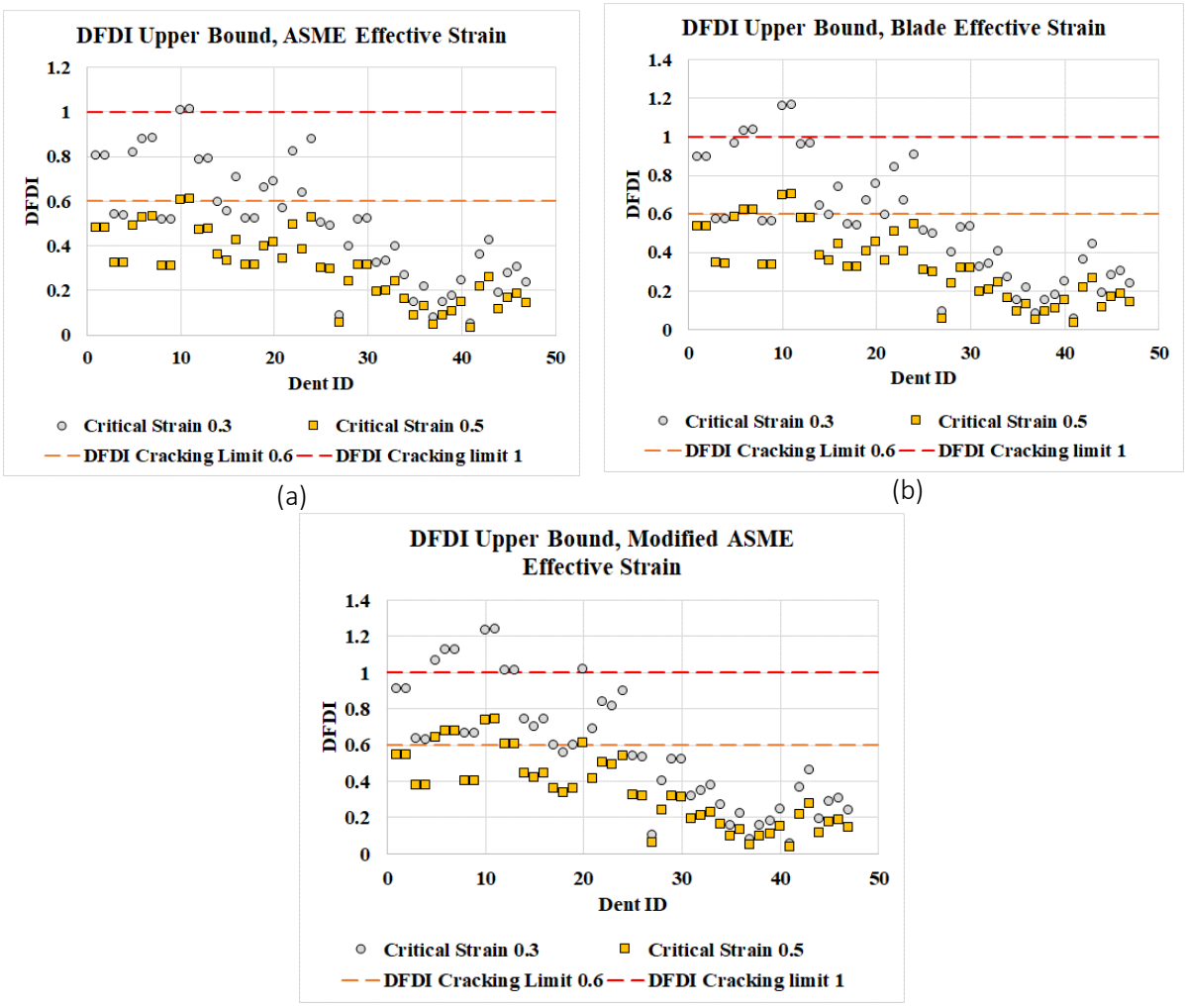

Figure 12 - DFDI index evaluated for full-scale test dents using (a) ASME strain (b) Blade Strain and (c) modified ASME strain

2.5.2. ASME B31.8 Limit Strain Criterion

ASME B31.8 provides a guideline stating that the likelihood of cracking is high if an indentation with strains exceeding 6% occurs [4] The effective strains (ASME, Blade and modified ASME) exceeding this limit suggests that the dent might have incurred cracking during indentation. This criterion was applied to the 47 full-scale dents. Thirty-two (32), 33 and 33 dents were predicted to have incurred cracking for ASME, Blade and modified ASME strains, respectively. None of the full-scale dents had cracks due to indentation. The ASME strain values of full-scale dents compared to the 6% strain limit, are presented in Figure 13.

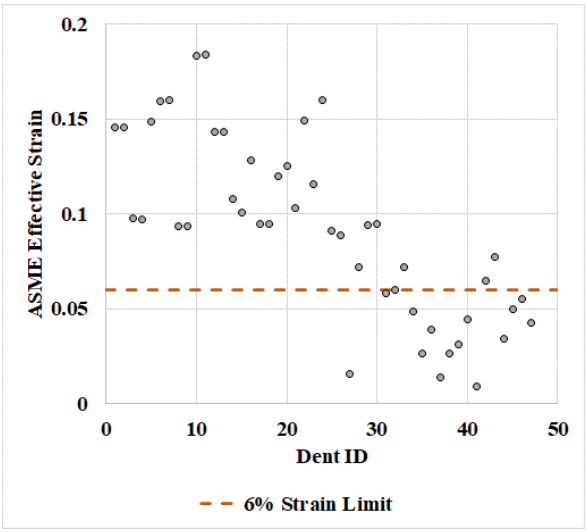

(a)

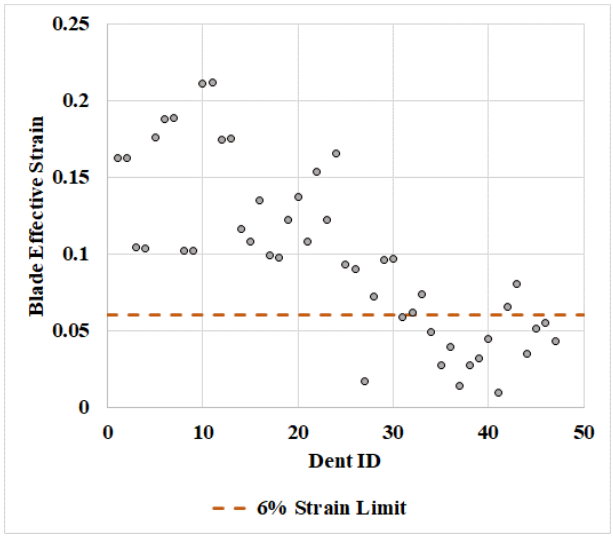

(b)

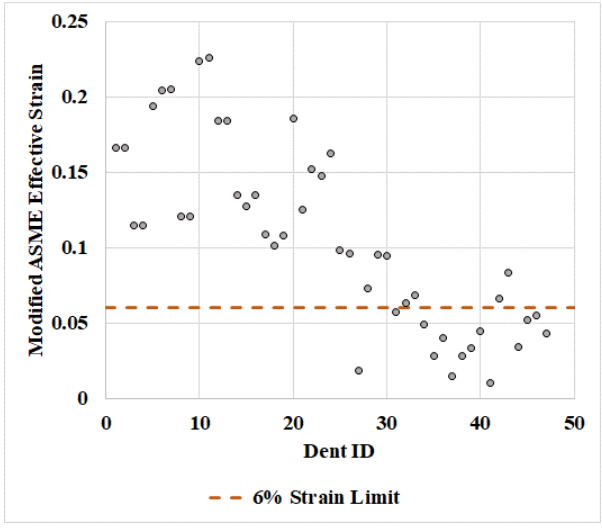

(c)

Figure 13 – ASME B31.8 limit strain cracking criteria evaluated for full-scale test dents using (a) ASME strain (b) Blade Strain and (c) modified ASME strain

2.5.3. Comparison of Cracking Effective Strain from DFDI and ASME Limit Strain Criteria

Upper bound DFDI criterion quantifies damage based on material property (critical strain) and indentation equivalent strain. The ASME B31.8 effective strain estimate from ILI data can be used as the equivalent strain, in the DFDI equation to back calculate limit strain and compare it with 6% limit strain as defined in ASME B31.8 Appendix R. Use of different critical strain (ε_0) values (0.3 to 0.5 for pipeline steels) and cracking DFDI limit (0.6 or 1), can produce a range of effective strain limits [3]. The evaluation of these limit strains is presented below.

$$DFDI_{Upper\ Bound} = \frac{1.65\varepsilon_{eq}}{\varepsilon_0}$$

$$Limit\ Strain = \frac{DFDI_{Upper\ Bound} \times \varepsilon_0}{1.65}$$

For example, for DFDI cracking limit of 0.6 and $\varepsilon_0 = 0.3$, the strain limit is given by,

$$\varepsilon_{eq} = \frac{0.6 \times 0.3}{1.65} = 0.11\ (11\%\ Limit\ Strain)$$

Similarly, using other combinations of critical strain and DFDI cracking limits, limit strain of up to 30% can be obtained. There is a large discrepancy between a 6% strain limit as defined in ASME B31.8 Appendix R and the range of 11% - 30% strain limit calculated from the DFDI methodology. This is the primary reason that a larger portion of full-scale test specimens show potential for cracking using ASME limit state of 6% as compared to the DFDI methodology.

3. EFFECTS OF VARIATION OF ILI DATA ON FATIGUE LIFE AND STRAIN ESTIMATION OF DENTS

The variation in ILI tool reported measurement of dent shape can introduce variations in fatigue life (PRCI Level 1 and Level 2, API RP 1183 [1]) and dent strain (ASME B31.8 [4]) estimation, as these models are dependent on the dent shape. This section is dedicated to the investigation of the sensitivity of these models to ILI measurement variability. This investigation was conducted by employing Monte Carlo simulations, where error distributions of the dent dimensions were sampled and applied to the dent profiles and the fatigue life and strain estimates were calculated from the randomized profiles. The collated data provides a measure of the variation observed in the fatigue life and strain estimates when the dent shapes are subjected to various error distributions. ILI in-service dent data was used for these simulations, and it consisted of about 900 dents, of 6 different pipe ODs (273 – 1066 mm/10-42 in) and a dent depth range from 0.25-11% OD.
In addition to the artificially induced errors, variation in estimates were also obtained from multiple ILI measurements of a set of dents which were part of ILI pull tests (PRCI NDE-4-18). Laser scan data for these dents was available and was used to calculate baseline fatigue life and dent strains. The fatigue lives and dent strains calculated from multiple measurements from different ILI Service Providers were compared against the estimates evaluated from laser scan dent geometry.

3.1. Variation of Dent Profiles

The first step in generating a family of variations of a dent for the Monte Carlo simulation was to sample percentage error values from normal distributions of percentage errors. These normal distributions were generated using the normal random number generator function, *normrnd*, in MATLAB [16]. The mean errors were all set at 0, while three different standard deviation values were considered, 10%, 15% and 20%. Six shape variation schemes were implemented which required six sets of error distributions. These involved the variation of depth, length, and width, individually, each with a standard deviation of 20%. The next three sets consisted of coupled variations of the three dimensions at 10%, 15% and 20% standard deviations (SD). For each distribution, a million samples were extracted. Hence for each dent, approximately 6,000,000 simulations were performed.

The application of percentage error to vary the dent profiles is illustrated in Figure 14. Based on an instance of percentage error from the distributions, the profiles were scaled in the manner illustrated in Figure 14. The dent peak of the axial and transverse profiles was offset to the origin and the axial length (length), transverse length (width) and deflection (depth) were scaled according to the respective percentage error instances. After the family of varied dent profiles had been generated based on the six randomization schemes, the dent geometry parameters (API 1183) and the dent peak curvatures were evaluated for each variation. These values were then used to calculate the fatigue life and strain distributions for each simulated dent shape variation. The percentage coefficient of variation (COV) was evaluated for the fatigue life and strain distributions. Coefficient of variation provides a means to quantify the sensitivity of the model to the ILI measurement errors, as it is an average measure of spread of the resulting distribution, normalized to the mean.

For both restrained and unrestrained dents, the fatigue life estimates were least sensitive to the scheme with only dent width variation (SD 20%), with an average COV of 7% and 12%, respectively. For both, the estimates were most sensitive to the scheme where all three dimensions were varied (SD 20%), with an average COV of 17% and 34%, respectively. With regards to variation of a single dimension, for both restrained and unrestrained dents, the estimates were most sensitive to depth

(SD 20%), with an average COV of 10% and 22%, respectively. The minimum and maximum COV of fatigue life estimates, observed for any restrained dent with any scheme, were 1% and 26%, respectively; 12% and 36%, respectively, for unrestrained dents. The ASME strain estimates were least sensitive to the scheme with only length variation (SD 20%), with an average COV of 19%. The estimates were most sensitive to the scheme where all three dimensions were varied (SD 20%), with an average COV of 48%. With regards to variation of a single dimension, the estimates were most sensitive to width (SD 20%), with an average COV of 37%. The minimum and maximum COV of ASME strain estimates, observed for any dent with any scheme, were 19% and 58%, respectively. Detailed results of the Monte Carlo simulations can be found in Ref [8]. COV values for a data set consisting of dents on 914 mm (36 in) OD pipes have been presented in Figure 15.

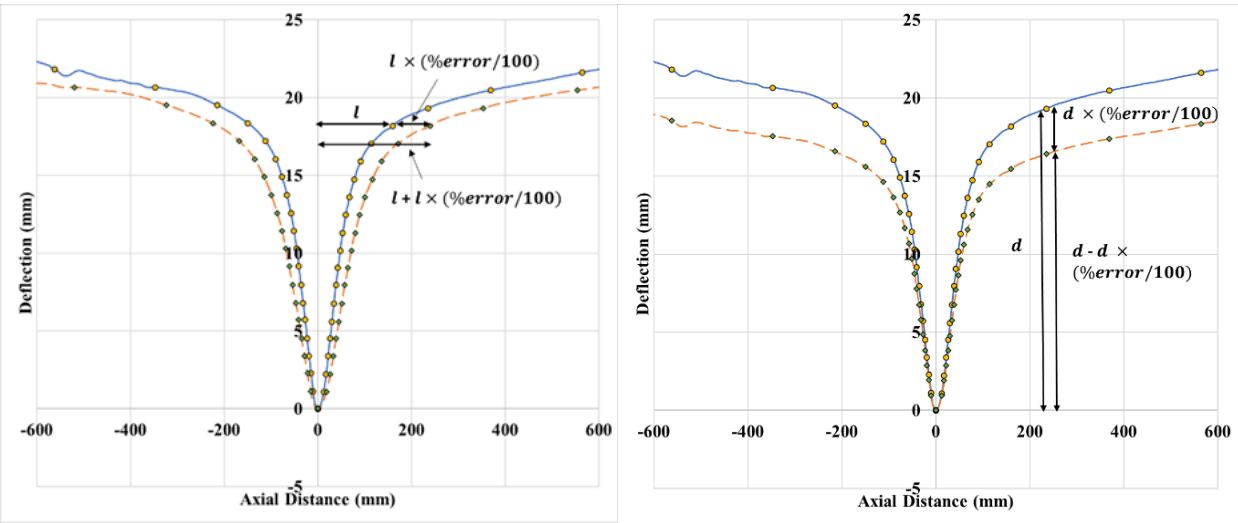

(a) (b)

Figure 14 - Illustration of variation of profile (a) length (b) depth, by application of percentage error

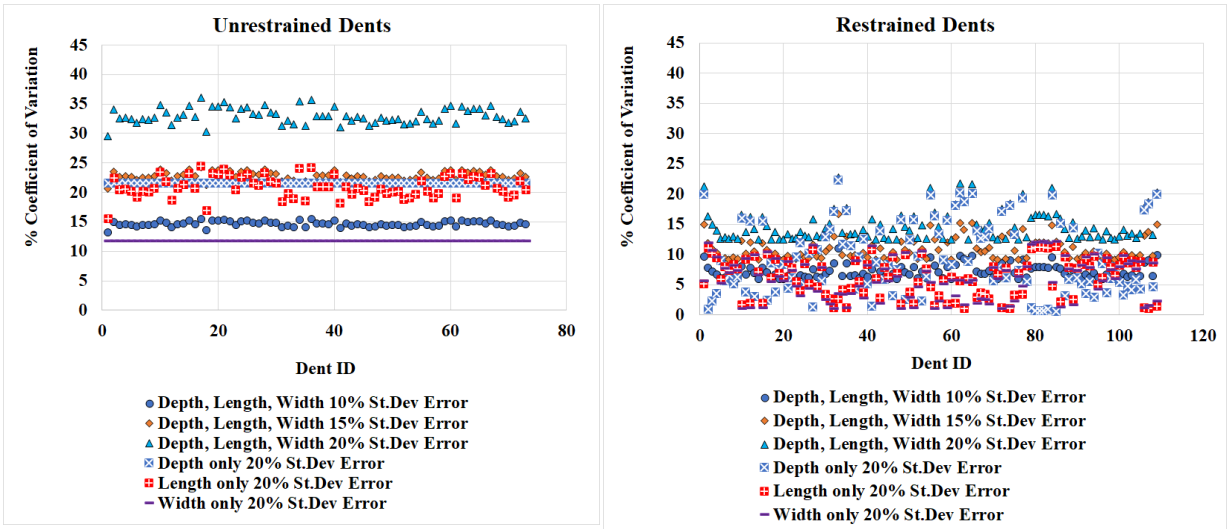

(a) (b)

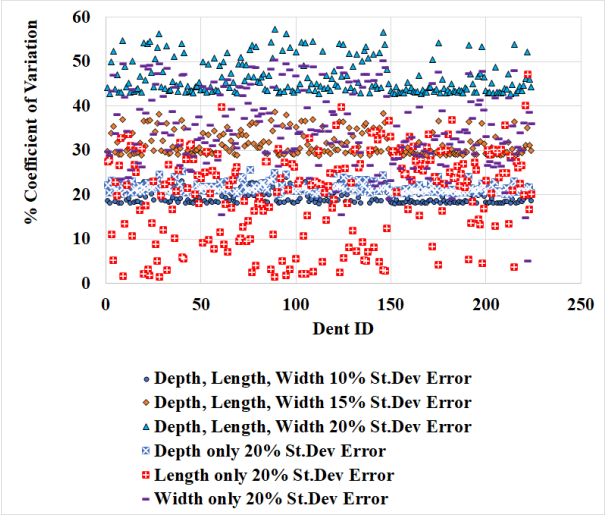

(c)

Figure 15 - Coefficient of variation of (a) unrestrained dent fatigue life distributions (b) restrained dent fatigue life distributions (c) ASME strain distributions, from a set of dents on 914 mm (36 in) pipe

3.2. Comparison of Fatigue Life and Strain Estimates Evaluated using Laser Scan and ILI Dent Geometry

As part of the PRCI NDE-4-18 project, a series of dents had been measured by multiple ILI service providers. Under the ILI trial program, each ILI vendor had to perform multiple passes of the pipe strings at different speeds. As a result, multiple measurements of the same dents by each ILI service provider were available. The dents had also been laser scanned and this data was taken as the reference data against which the ILI data could be compared. Data from 53 single peak dents were employed for this analysis and each dent had up to 50 ILI measurements, providing a sizable family of variations for each dent. This provided a substantial empirical data set with which the effect of variation of dent profiles on fatigue life and strain estimates could be studied. This data, along with the laser scan data of the dents was used to evaluate fatigue life and strain estimate distributions. The standard deviation of percentage errors (calculated with respect to the laser scan reference data) were evaluated for the fatigue life and strain estimates, as a measure of spread of the estimated values. It was observed that the standard deviation values were mostly within 40% and 60% for fatigue life and strain estimates (Figure 16), respectively, which fall well within the range of coefficient of variation values from Monte Carlo simulations, representing good agreement between the two approaches.

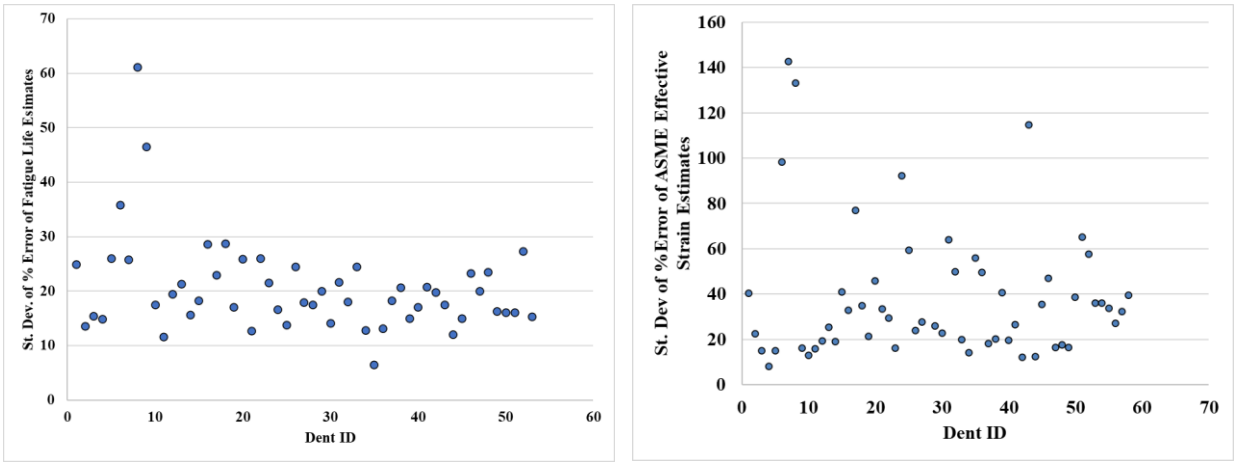

(a) (b)

Figure 16 - Standard deviation of %error of (a) fatigue life (b) ASME effective strain, from pull trials

4. DENT FATIGUE LIFE ASSESSMENT SAFETY QUANTIFICATION

The objective of this task was to ascertain safety factors (model bias) that are inherent in the dent fatigue life estimation of plain dents and dents interacting with coincident features. This was accomplished by defining scale factors (s) that can be applied to the calculated fatigue lives to return life estimates that have minimum factors of safety (R) with a specified certainty (α). These scale factors were evaluated by comparing experimental full-scale dent fatigue life data with the estimates from the fatigue life assessment methodologies developed under PRCI and CEPA sponsored research and incorporated in API RP 1183 [1][17]. Histograms of the ratio of experimental to predicted fatigue lives (safety factor) were developed and continuous probability distribution functions were fitted onto these. These functions provided estimates of the probability of the safety factor being above certain values. These fitted probability density functions were scaled so that a minimum factor of safety, with a specified certainty, could be achieved and the factor by which these functions were scaled are denoted as scaling factors. The evaluated scaling factors can be used to scale the estimated fatigue life to ensure that a minimum amount of factor of safety can be ensured with a specified amount of certainty, for a particular fatigue life assessment methodology.

The first step in developing the scale factors was to compare experimental fatigue lives with estimates from various fatigue life assessment methodologies. For this purpose, data from 127 full-scale dent fatigue life tests was used. Out of the 127 dents, there were 61 plain dents, 29 dents interacting with metal loss and 37 dents interacting with welds (girth welds and long seam welds). Twenty-four (24) dents out of the total of 127 dents were field dents removed from in-service pipelines and the rest were created in the laboratory. The pipe ODs ranged from 273 to 1016 mm (10 to 42 in). The dents were created using indenters of wide-ranging geometry. Please refer to Ref [8] for more detail. The dent and pipe geometry data from these dents formed in the full-scale trials were used along with the associated pressure range data to predict the number of cycles to failure (N_{pred}) using the dent fatigue life models. Additionally, appropriate life reduction factors were applied to the predicted cycles as recommended in API RP 1183, for interaction with metal loss and welds. The predicted fatigue lives were compared with the experimental number of cycles to failure (N_{exp}). The life predictions were made using three different dent fatigue life prediction models described in API RP 1183 – Level 0 (Section 7.4.2), Level 0.5 (Section 7.4.3) and Level 2 (Section 8.3.4). The BS 7608 Class D Mean (Level 0 and 0.5) and Mean -1sd (Level 2) SN curves were used to calculated the fatigue lives. The ratio of experimental to predicted number of cycles to failure (r) was calculated for each prediction model. This ratio is the multiple by which the experimental lives are greater than the predicted lives i.e., modeling bias. Histograms of r were generated and lognormal statistical distributions were fitted onto them. The three fatigue life assessment methodologies were applied to plain dents, dents interacting with metal loss and welds. Figure 17 shows the fitted r histogram for Level 0, 0.5 and 2 fatigue analyses of plain dents. The lognormal distributions were modified by applying scale factors (s) such that the resulting distribution of effective ratios of experimental to predicted fatigue life (r') may be used to define Target Safety Factors (R) for defined confidence levels (α). A schematic representation of the scaling of the lognormal distribution has been presented in Figure 18.

$$r = \frac{N_{exp}}{N_{pred}} \tag{13}$$

$$r' = \frac{N_{exp}}{N_{pred}'} = \frac{N_{exp}}{N_{pred}/_{S}} = \frac{N_{exp}}{N_{pred}} * s = r * s \tag{14}$$

Where, r is the ratio of experimental to predicted number of cycles to failure, N_{exp} is the experimental number of cycles to failure, N_{pred} is the predicted number of cycles to failure, $N_{pred}{}'$ is the effective predicted number of cycles to failure, r' is the effective ratio of experimental to

predicted number of cycles to failure and $\mathbf{s}$ is the scale factor which when applied to N_{pred} can result in r' greater than a specified target safety factor (R). The level of confidence that $r' > R$ is given by α, which is the probability of exceedance of R in the r' probability distribution (scaled lognormal distribution).

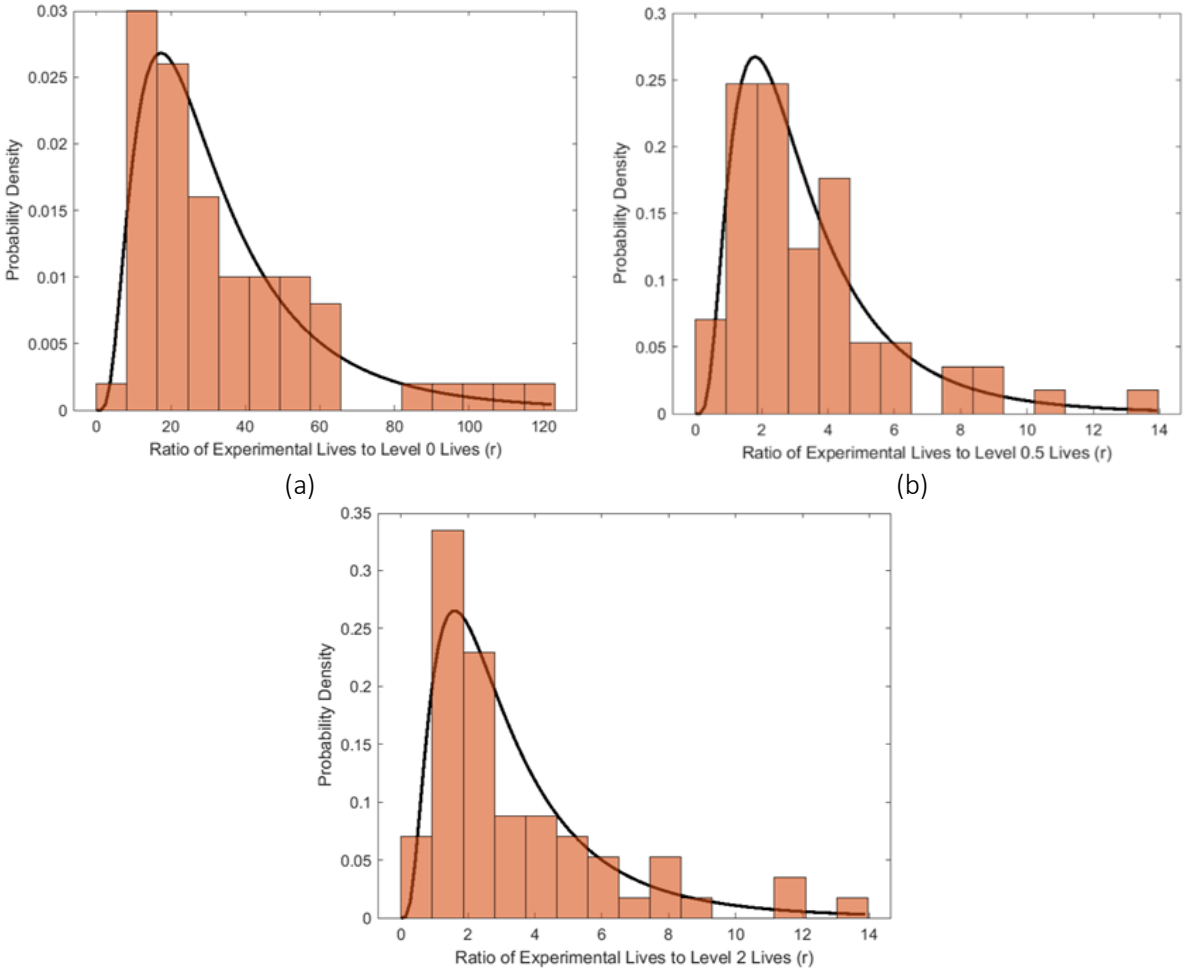

Figure 17 – Fitted *r* ratio distributions of (a) Level 0, Mean (b) Level 0.5, Mean and (c) Level 2 Mean - 1sd, fatigue life estimation criteria, for plain dents

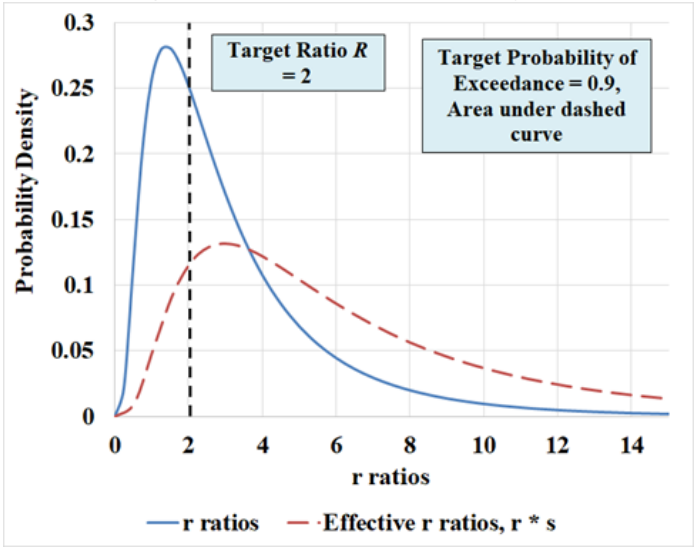

Figure 18 – Sample probability distribution function and scaled probability distribution function of *r* ratios

Some of the scaling factors evaluated for different fatigue life estimation models and for different dent interaction conditions at 80% certainty have been presented in Table 2. For a particular fatigue life estimation model, the scaling factor value required to obtain a minimum safety factor of *R*, with 80% certainty, can be obtained from Table 2 and applied to calculated fatigue life estimate as shown below.

$$N_{pred}{}'(for\ r > R, with\ certainity\ \alpha) = \frac{N_{pred}}{s} \tag{15}$$

For example, if a factor of safety of 2 at 80% certainty needs to be ensured for a Level 2, Mean -1sd, fatigue life estimate (N_{pred}) of a dent interacting with metal loss, then a scaling factor of 1.02 must be applied to N_{pred} as shown in Equation 15.

Scaling Factor Matrices				
	Level 0, Mean			
	Probability of Exceedance of Target Safety Factor α = 0.8			
Target Safety Factor (R)	Plain Dents	Dents Interacting w/ Metal Loss	Dents Interacting w/ Weld. Reduction Factor = 10	Dents Interacting w/ Weld. Reduction Factor = 5
10	1	1	1	1
15	1	1	1	1
25	1.6	1.22	1	1
	Level 0.5, Mean			
	Probability of Exceedance of Target Safety Factor α = 0.8			
Target Safety Factor (R)	Plain Dents	Dents Interacting w/ Metal Loss	Dents Interacting w/ Weld. Reduction Factor = 10	Dents Interacting w/ Weld. Reduction Factor = 5
2	1.25	1	1	1
3	1.88	1.04	1	1
6	3.76	2.08	1	1.05
	Level 2, Mean -1sd			
	Probability of Exceedance of Target Safety Factor α = 0.8			
Target Safety Factor (R)	Plain Dents	Dents Interacting w/ Metal Loss	Dents Interacting w/ Weld. Reduction Factor = 10	Dents Interacting w/ Weld. Reduction Factor = 5
2	1.36	1.02	1	1
3	2.04	1.53	1	1
6	4.08	3.07	1	1.1

Table 2 - Sample scaling factors associated with level 0, 0.5 and 2 dent fatigue life assessment

Level 0 is the most conservative screening method, it can be seen that large safety factors can be assured with 80% certainty without the application of scaling factor to the life prediction. Also, the recommended life reduction factor of 10 for weld interaction results in high conservatism as no scaling is required for all the listed safety factors, across all prediction methods. This suggests that the reduction factor is too conservative and the use of a lower value, like 5, may prove more appropriate.

The results for a life reduction factor of 5 due to dent weld interaction have also been presented in Table 2. As expected, the scaling factors are higher for the Level 2 method as it is the least conservative. For more detailed safety factor quantification results, please refer to Ref [8].

5. CONCLUDING REMARKS

The present study builds on mechanical damage (MD) assessment and management tools, developed over several years and incorporated in API RP 1183 [1]. The current project enhances previously developed tools being adopted in an industry recommended practice (API RP 1183) for pipeline MD integrity assessment and management. Three main tasks of the project were to assess and improve the indentation strain prediction models, to assess the effect of ILI data variability on fatigue life and strain estimations and to develop safety factors regarding fatigue life estimation.

With regard to indentation strain, two strain estimation models (ASME and Blade) were assessed against a large FE database. ASME strains estimates diverged for deep (>= 6% OD) and sharp dents (<= 200 mm/8 in radius of curvature). Modifications were suggested for ASME model by improving axial and adding circumferential membrane strain formulation. The modified ASME and Blade strains compared well against the FE strains. A prediction model was also developed to predict indentation strains for unrestrained dents for ASME and BMT Modified ASME formulations. Two dent cracking criteria, DFDI and ASME B31.8 Limit Strain, were also assessed against dent full-scale test data. Based upon the least conservative and the most conservative options, 0 out of 47 or 16 out of 47 tests were predicted to have cracks during indentation based on Blade formulation, respectively. Strain limit criterion of 6% in ASME B31.8 Appendix R was found to be very conservative as 32 out of 47 tests exceeded the 6% strain limit.

With regard to assessing the effect of ILI measurement variability on fatigue life and strain estimation models, two approaches were adopted. The first was to perform Monte Carlo simulations on in-service dent ILI data, where errors were introduced to the profile to create families of variations of each dent. Fatigue life and strain estimate distributions were evaluated from these variations and a measure of spread in form of coefficient of variation were calculated. The coefficient of variation of fatigue life estimates ranged from 1-36%, while for strains it ranged from 19-58%. The second approach was to extract the variations in fatigue life and strain estimates from pull trials data. The distributions evaluated from the pull trials agreed well with the Monte Carlo simulations as the standard deviations of % error of these dents were found to be mostly within upper bounds of the Monte Carlo simulation results.

Quantification of safety factors associated with fatigue life estimation methods provided in API 1183 was accomplished by compiling safety factor histograms using full-scale dent experimental and estimated fatigue life values. Lognormal probability distributions were fitted onto the safety factor histograms and these distributions were scaled to achieve the required safety factor at a specified probability of exceedance. The process was carried out for fatigue life estimation for plain dents, dents interacting with welds and dents interacting with corrosion.

6. REFERENCES

[1] American Petroleum Institute: *API RP 1183, Assessment and Management of Dents in Pipelines*. API, 2020.

[2] R. W. Revie, *Oil and Gas Pipelines: Integrity and Safety Handbook*. John Wiley & Sons, 2015.

[3] U. Arumugum, M. Gao and R. Krishnamurthy: *Study of a Plastic Strain Limit Damage Criterion for Pipeline Mechanical Damage Using FEA and Full-Scale Denting Tests.* International Pipeline Conference, 2016.

[4] American Society of Mechanical Engineers: *ASME B31.8-2018, Gas Transmission and Distribution Piping System*. ASME, 2018.

[5] M. Gao, R. McNealy, R. Krishnamurthy and I. Colquhoun: *Strain-Based Models for Dent Assessment – A Review.* ASME 7th International Pipeline Conference, 2008.

[6] S. A. Lukasiewicz, J. A. Czyz, C. Sun and S. Adeeb: *Calculation of Strains in Dents Based on High Resolution In-Line Caliper Survey.* ASME 6th International Pipeline Conference, 2006.

[7] M. J. Rosenfeld, P. C. Porter and J. A. Cox: *Strain Estimation Using Vecto Deformation Tool Data.* ASME 2nd International Pipeline Conference, 1998.

[8] A. Rana, S. Tiku and A. Dinovitzer: *Improve Dent/Cracking Assessment Methods MD5-2*. PRCI Catalog No. PR-214-203806-R01.

[9] S. Tiku: *Management of Dents*. CEPA, 2021.

[10] S. Tiku: *Full Scale Fatigue Testing of Dents (Plain Dents and Dents Interacting with Welds and Metal Loss) MD4-2.* PRCI Catalog No. PR-214-073510-R01, 2018.

[11] S. Tiku: *Full Scale Testing of Interactive Features for Improved Models.* US DOT PHMSA DTPH56-14-H-00002, 2017.

[12] S. Tiku: *Full Scale Testing of Shallow Dents with and without Interacting Features MD4-14*. PRCI Catalog No. PR-214-163714, 2019.

[13] E. A. de Souza Neto, D. Perić and D. R. J. Owen: *Computational Methods for Plasticity: Theory and Applications*. John Wiley & Sons, 2008.

[14] MATLAB: *Solve Nonlinear Least-Squares (Nonlinear Data-Fitting) Problems.* [Online]. Available: www.mathworks.com/help/optim/ug/lsqnonlin.html. [Accessed 7 September 2020].

[15] M. Gao, R. Krishnamurthy, S. Tandon and U. Arumugum: *Critical Strain Based Ductile Damage Criterion and its Application to Mechanical Damage in Pipelines.* 13th International Conference on Fracture, 2013.

[16] MATLAB: *Normal random numbers.* [Online]. Available: https://www.mathworks.com/help/stats/normrnd.html. [Accessed 2 1 2022].

[17] S. Tiku: *Fatigue Life Assessment of Dents with and without Interacting Features MD4-9.* PRCI Catalog No. PR-214-114500-R01.